Lumbricus Erythrocruorin at 3.5 Å Resolution: Architecture of a Megadalton Respiratory Complex

William E. Royer, Jr.,[1,2,*] Hitesh Sharma,[1,3]
Kristen Strand,[1,4] James E. Knapp,[1]
and Balaji Bhyravbhatla[1]
[1] Department of Biochemistry and Molecular
   Pharmacology
University of Massachusetts Medical School
Worcester, Massachusetts 01655

Summary

Annelid erythrocruorins are highly cooperative extracellular respiratory proteins with molecular masses on the order of 3.6 million Daltons. We report here the 3.5 Å crystal structure of erythrocruorin from the earthworm *Lumbricus terrestris*. This structure reveals details of symmetrical and quasi-symmetrical interactions that dictate the self-limited assembly of 144 hemoglobin and 36 linker subunits. The linker subunits assemble into a core complex with D_6 symmetry onto which 12 hemoglobin dodecamers bind to form the entire complex. Although the three unique linker subunits share structural similarity, their interactions with each other and the hemoglobin subunits display striking diversity. The observed diversity includes design features that have been incorporated into the linker subunits and may be critical for efficient assembly of large quantities of this complex respiratory protein.

Introduction

Assembly of functional units into large macromolecular complexes permits greater coordination and regulation in many biological processes. Design of large macromolecular complexes often involves symmetrically arranged subunits. Symmetrical assemblages require surfaces used for subunit interactions to be fully satisfied in order to prevent unwanted further assembly, thus ensuring such biological assemblies are limited to a discrete size. This can be achieved by the use of one of the closed point symmetry groups—cyclic, dihedral, tetrahedral, octahedral, or icosahedral. However, for a number of assemblages, the symmetry expressed in these point groups does not suffice for the quantity of subunits present. Noteworthy examples include spherical viruses that are commonly arranged with icosahedral symmetry, but most often contain many more subunits than can be accommodated by the 60 equivalent icosahedral symmetry positions. Caspar and Klug (1962) proposed an elegant solution to this problem with the principle of quasi-equivalence, in which chemically identical subunits occupy nearly equivalent positions with only slightly altered bonding patterns. Quasi-equivalence remains an important theoretical underpinning of our understanding of spherical virus construction, although viral subunits have shown substantially greater bonding variations than originally envisioned (Harrison, 2001).

Symmetrical arrangements of multiple subunits are also observed in invertebrate giant extracellular respiratory proteins. These include the copper-containing hemocyanins, from arthropods and mollusks (van Holde and Miller, 1995), and heme-containing respiratory proteins, such as those found in annelid worms. The most prevalent of these annelid complexes are known as either erythrocruorins or hexagonal bilayer hemoglobins. Our designation of these proteins as erythrocruorins emphasizes the requirement of nonhemoglobin linker subunits for assembly (Kuchumov et al., 1999; Lamy et al., 2000; Zhu et al., 1996) and their similar overall architectures to those of annelid chlorocruorins (de Haas et al., 1996a, 1997; Schatz et al., 1995). Because of their extracellular nature and giant size, erythrocruorins were important subjects for seminal biophysical investigations. *Lumbricus* erythrocruorin was the first protein ever reported to be crystallized, in 1840 by Hünefeld (McPherson, 1999), one of the first proteins investigated in Svedberg's initial ultracentrifugation experiments (Svedberg and Ericksson-Quensel, 1933), and an early molecular subject of electron microscopy (Roche et al., 1960). Both erythrocruorins and chlorocruorins display overall D_6 dihedral symmetry; similarly to icosahedral viruses, however, many more subunits are present than can be accommodated in the 12 equivalent D_6 symmetry positions.

A number of biological advantages arise from the formation of the giant erythrocruorins. Such large complexes can be readily retained as freely dissolved entities in the vascular system and each complex can be endowed with a very large oxygen binding capacity. Moreover, subunits can be arranged in a manner to permit intersubunit communication that can result in cooperative oxygen binding along with additional regulatory features that promote efficient oxygen transport. In the case of *Lumbricus* erythrocruorin, highly cooperative oxygen binding (Hill coefficient = 7.9, under conditions of maximum cooperativity) is coupled with the binding of cations and protons (Fushitani et al., 1986). Due to their large size, extracellular nature, and resistance to oxidation (Dorman et al., 2002; Harrington et al., 2000), erythrocruorins have been proposed as useful model systems for developing therapeutic extracellular blood substitutes (Hirsch et al., 1997; Zal et al., 2002).

Our previous 5.5 Å resolution crystal structure of *Lumbricus* erythrocruorin revealed an architecture of 144 hemoglobin subunits arranged into 12 dodecamers that assemble onto a central scaffold of 36 linker subunits (Royer et al., 2000). This has been complemented by a 2.6 Å resolution crystal structure of purified hemoglobin dodecamers (Strand et al., 2004). We report here the crystal structure of the entire *Lumbricus* erythrocruorin molecule at 3.5 Å resolution. Our results, which, to our

*Correspondence: william.royer@umassmed.edu
[2] Lab address: http://www.umassmed.edu/bmp/faculty/royer.cfm
[3] Present address: Department of Molecular Biophysics and Biochemistry, Yale University, New Haven, Connecticut 06511.
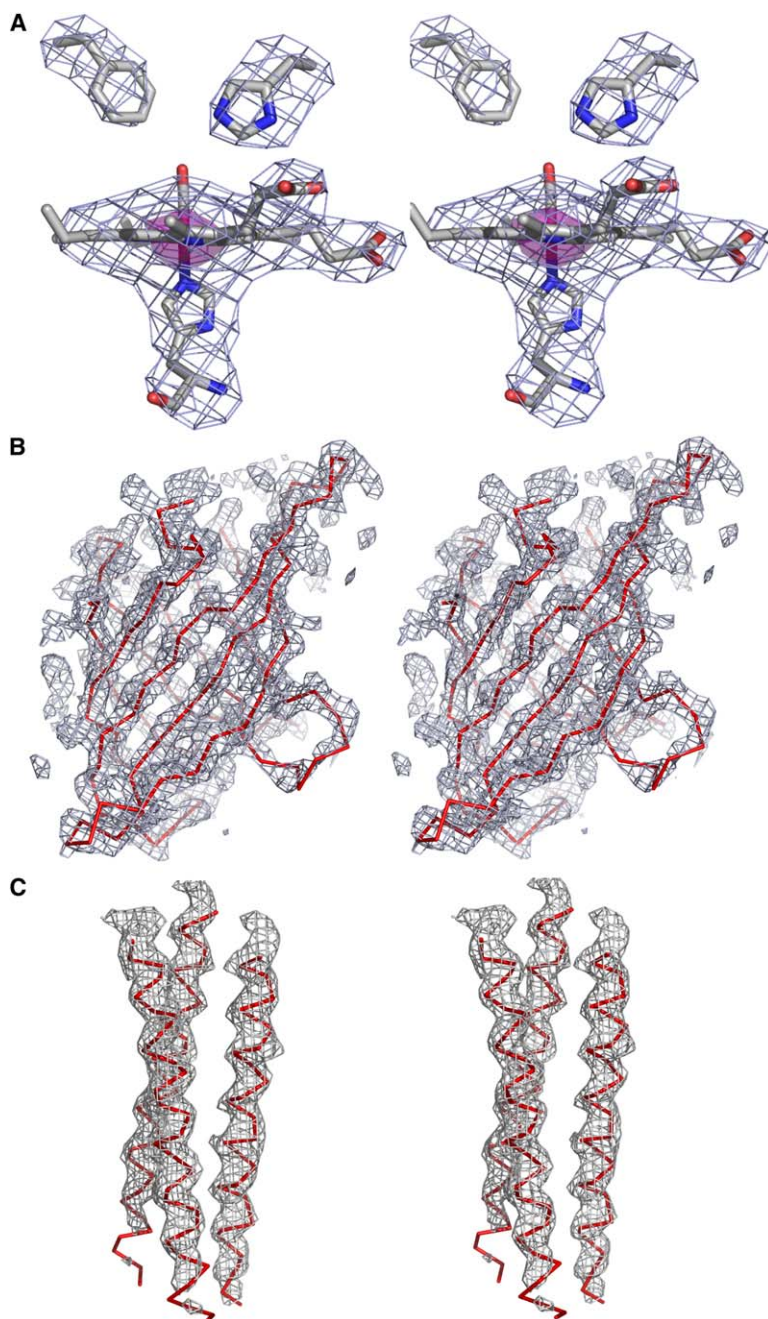[4] Present address: Genzyme Corporation, Cambridge, Massachusetts 02142.

Figure 1. Stereodiagrams of 24-Fold Averaged Electron Density Maps for *Lumbricus* Erythrocruorin

(A) The heme region for one hemoglobin subunit *a* is shown with gray contours at 1.5σ and magenta surface at 12σ around the heme iron position. Included with the density are atomic models for the heme group, proximal histidine (F8), distal histidine (E7), and B10 Phe.
(B) An α-carbon trace (red) for the β barrel domain of L1 is shown with electron density at a contour level of 3σ superimposed.
(C) An α-carbon trace (red) for the linker triple-stranded coiled coil is shown with electron density contoured at 3σ. The density for the coiled coil shows the course of the helices, but poorer density for the amino termini at the bottom and side chains (compare with middle panel) is consistent with high refined group B factors suggesting high mobility for this portion of the linker structures.

knowledge, provide the first complete set of atomic models for an entire megadalton complex from this class of respiratory proteins, reveal the central role of interactions among three distinct linker subunits to dictate the intricate hierarchy of symmetry of these complexes.

Results

Growth of a new triclinic crystal form of *Lumbricus* erythrocruorin permitted the determination of this structure to 3.5 Å resolution. As described in Experimental Procedures, the starting point for phasing the new diffraction data was the 5.5 Å electron density maps obtained from orthorhombic crystals grown in 1.8 M phosphate. Using molecular averaging for phase extension,

we were able to obtain a readily interpretable map, portions of which are shown in Figure 1. An atomic model, including two whole molecules (7.2 million Daltons) per asymmetric unit, has been refined to a conventional R factor of 0.288 and to a free R of 0.297. Crystallographic statistics are provided in Table 1.

Overall Structure
Lumbricus erythrocruorin is assembled from 180 polypeptide chains into an overall hexagonal bilayer shape (Figure 2). The vertices of two hexagonal halves of the molecule are partially staggered, with one half rotated about the 6-fold axis by about 16° from an eclipsed arrangement, as was evident from cryo-electron microscopic investigations (de Haas et al., 1997; Schatz et al.,

Table 1. Crystallographic Statistics

Crystal Parameters	
Space group	P1
a (Å)	176.08
b (Å)	257.96
c (Å)	436.53

Data Collection	
Resolution range (Å)	100–3.5
Highest shell (Å)	3.63–3.5
Total observations	1,718,296
Unique reflections	890,862
Completeness (%)	89.3 (74.9)[a]
$<I/\sigma(I)>$	8.4 (2.0)[a]
R_{merge} (%)	7.8 (35.4)[a]

Refinement	
R factor (%)	0.288
Free R factor (%)	0.297
Resolution range (Å)	50.0–3.5
Number of atoms	
Protein	458,544
Heme and CO ligand	12,960
Calcium	96
Zinc	24
Rms deviation from ideal	
Bond length (Å)	0.009
Bond angles (°)	1.22
Average B factors (Å^2)	
Protein main chain	61.0
Protein side chain	77.5
Heme and CO	54.6
Calcium	25.7
Zinc	58.3
Ramachandran statistics	
Most favored region (%)	85.0
Additional allowed region (%)	13.9
Generously allowed region (%)	1.1
Disallowed region (%)	0.0

[a] Values in parentheses refer to the highest resolution shell.

1995). Perpendicular to the 6-fold axis of this D_6 symmetric molecule are molecular dyad axes every 30°, alternating between two unique axes designated "Q" and "P" (Figure 2). This overall arrangement is dictated by a central core formed from 36 linker subunits which acts as a scaffold for binding 12 hemoglobin dodecamers.

Lumbricus erythrocruorin exhibits dihedral D_6 symmetry, in which each of 12 protomers is comprised of 12 hemoglobin subunits and three linker subunits (two protomers are shown in Figure 2C). Each protomer has an overall mushroom-like shape with a cap formed from the 12 hemoglobin subunits and a heterotrimeric linker head group, while the stem is formed by a triple-stranded coiled coil from the amino-terminal portion of the three linker subunits.

Hemoglobin Dodecamer Structure
The 144 oxygen binding hemoglobin subunits associate into 12 identical dodecameric units, with each dodecamer possessing a local 3-fold axis of symmetry. The dodecamer is assembled from three copies each of four unique hemoglobin subunits designated *a*, *b*, *c*, and *d* (Fushitani et al., 1988) or A1, A2, B1, and B2 (Bailly et al., 2002), with this latter designation based on comparison with other extracellular annelid hemoglobin se-

quences. Chains *a* (B2), *b* (A1), and *c* (B1) are disulfide linked into a heterotrimer, whereas chain *d* (A2) is not disulfide linked with any other subunits. All hemoglobin subunits contain an intrasubunit disulfide bond. Each dodecamer is arranged with three *d* chains clustering near the local 3-fold axis and three disulfide-linked *abc* trimers in an extended arrangement around the dodecamer's periphery (Figure 3). This gives rise to an overall domed shape, with the *d* chains at the apex of the dome forming a concave surface that interacts with the linker subunits. All hemoglobin subunits are involved in EF dimer pairing, in which an extensive dimeric interface forms from contacts involving the E and F helices and heme groups; EF dimer pairing has been found in all cooperative invertebrate hemoglobins investigated to date (Royer et al., 2005). Two types of EF dimers are observed: one formed from the pairing of *a* and *d* subunits and one from the pairing of *b* and *c* subunits of different disulfide-linked *abc* trimers. The structure of the dodecamer within the whole molecule of *Lumbricus* erythrocruorin is very similar to that obtained from the 2.6 Å crystal structure reported earlier for isolated dodecamers (Strand et al., 2004). (Superposition of 1743 α-carbon atoms from the isolated dodecamer structure with one dodecamer of the erythrocruorin structures yields a root-mean-square [rms] difference of 0.8 Å.) Our present structure reveals interactions of these dodecamers with linker subunits to form the complete erythrocruorin structure.

Individual Linker Subunit Structure
Three distinct linker subunits are present within each one-twelfth protomer, each of which shows a similar tertiary structure (Figure 4). The electron density maps allow unambiguous assignment of two linker subunits, designated L1 and L2, based on their known sequences (Kao et al., 2006). The third subunit within each one-twelfth subunit appears to be predominately L3, but L4 subunits may occupy this position within a small number of the one-twelfth subunits. (L3 and L4 have similar sequences.) This is consistent with characterizations of linker constituents that indicate L4 is only a minor component, less than one quarter of the abundance of L3 (Fushitani et al., 1996). We have therefore modeled the third linker chain within each one-twelfth protomer using the sequence of L3, and will refer to this subunit as L3.

The amino acid sequence of L2 contains both a glycine-rich N-terminal extension and an aspartate/histidine-rich C-terminal extension relative to the L1, L3, and L4 sequences (Figure 4) (Kao et al., 2006). No density is observed in our maps for either extension, although density for a few additional residues of L2 compared with the C terminus of L1 and L3 is apparent (Figure 4). Both the N and C termini project toward the center of the whole molecule where large solvent-filled space is available that could accommodate these extensions.

Each linker subunit is comprised of four motifs (Figure 4). Following several disordered residues at the amino terminus, the observed structure commences with a long α helix (21–30 residues). This α helix interacts with those from the two other linker subunits within a trimer to form a triple-stranded coiled coil. The long helix is followed by a nonhelical region (1–7 residues) and then
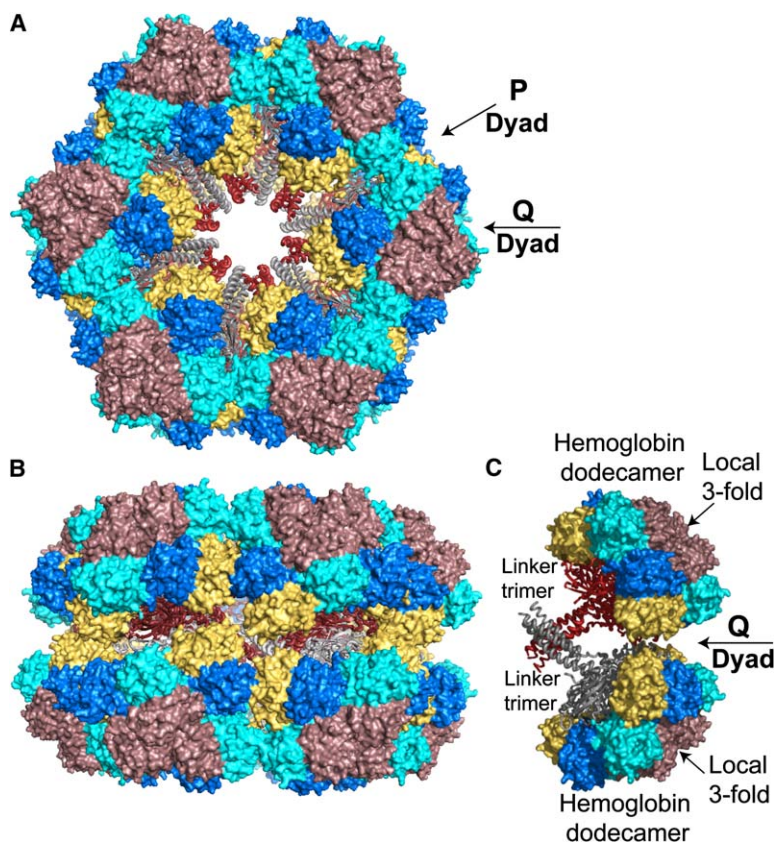
A

P
Dyad

Q
Dyad

B

C

Hemoglobin dodecamer

Local 3-fold

Linker trimer

Q
Dyad

Linker trimer

Local 3-fold

Hemoglobin dodecamer

Figure 2. *Lumbricus* Erythrocruorin Whole Molecule

(A) View along the molecular 6-fold axis. Hemoglobin subunits, at the outside of the molecule, are shown in a surface representation with *a* subunits in cyan, *b* subunits in dark yellow, *c* subunits in blue, and *d* subunits in dark purple. The course of polypeptide chains for linker subunits, in the interior of the molecule, is shown in red and gray for the two halves of the molecule.

(B) The whole molecule viewed along a P-dyad, rotated by 90° about the horizontal Q-dyad from the top view.

(C) Two one-twelfth units in the same orientation as in (B). Each one-twelfth unit includes a hemoglobin dodecamer and a linker heterotrimeric unit (red and gray). A local 3-fold relates three hemoglobin tetramers in the hemoglobin dodecamer and is coincident with a quasi-3-fold axis in the linker head region.

a shorter helix (12–17 residues) which participates in a short coiled coil within the head group of the linker heterotrimer. Subsequently, there is a cysteine-rich "LDL-A" module (39–41 residues), which is homologous with domains first found in the low-density lipoprotein (LDL) receptor, and an eight-stranded antiparallel β barrel domain (124 residues). Except for the long N-terminal helix, the linker subunits can be readily superimposed. L1 and

L2 are the most similar, with an rms difference of 1.6 Å for superposition of 182 α-carbon atoms (excluding the long N-terminal helix), whereas alignment of L3 yields an rms difference of 2.5 Å with L1 (176 pairs) and 2.1 Å with L2 (179 pairs).

The N-terminal triple-stranded coiled coils that project from each protomer toward the molecular center were clearly evident even at 5.5 Å resolution (Royer et al.,
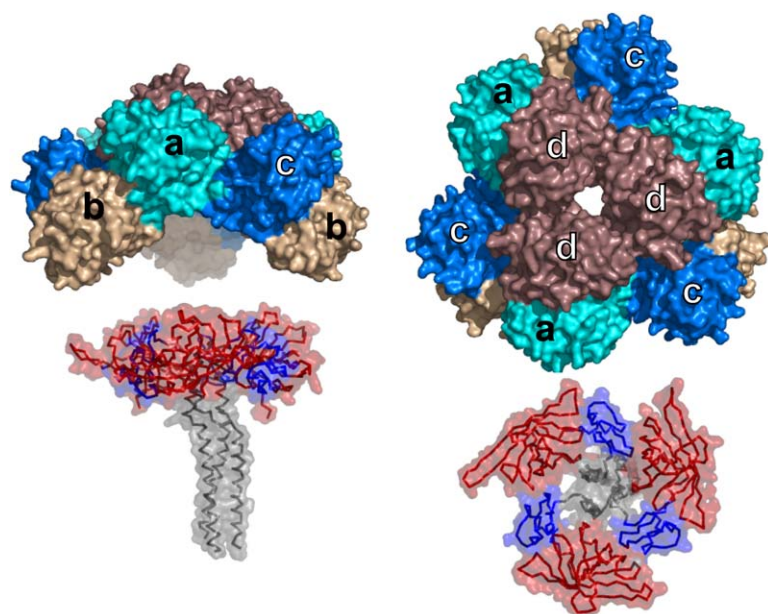

a
b
a
c
b

c
a
d
d
a
c
d
c
a

Figure 3. Linker Heterotrimer and Hemoglobin Dodecamer

The linker heterotrimer is shown as an α-carbon trace with a transparent surface for the entire heterotrimer with the helices colored gray, LDL-A module colored blue, and C-terminal β barrel domain in red. The hemoglobin dodecamer is shown in a surface representation with subunits colored as in Figure 1, except for the *b* subunits, which are shown as light brown. Both the dodecamer and linker heterotrimer are in the same orientation, but have been separated to reveal the contacting surfaces. On the left, the local 3-fold is vertical, whereas on the right, the view is along this 3-fold. Note the irregular 3-fold symmetric domed shape of the dodecamer that nestles against the quasi-3-fold symmetric outer surface of the head region of the heterotrimer, making extensive contacts with the β barrel (red) and LDL-A (blue) domains. Association of the dodecamer and heterotrimer results in a hollow spherical shaped mass arrangement.
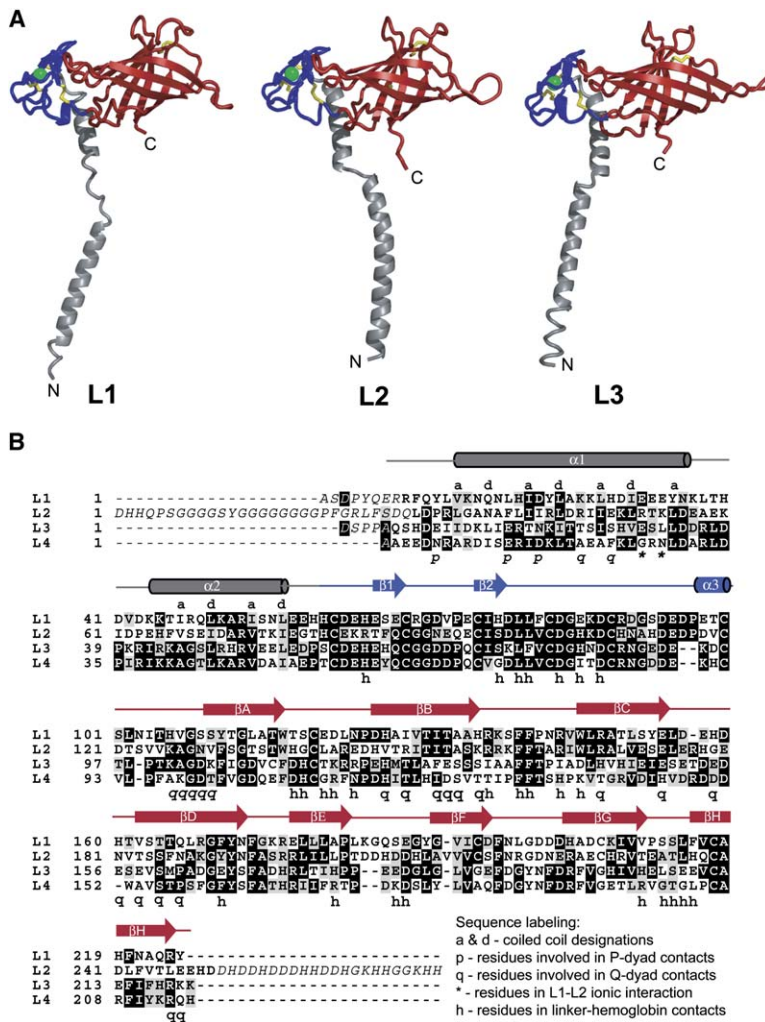
Figure 4. Structures and Sequences of the Linker Subunits

(A) Ribbon diagrams for the three unique linker subunits, with N and C termini as shown. Each linker subunit has a long α helix followed by a shorter α helix (both in gray), then a cysteine-rich LDL-A module (blue) and an eight-stranded β barrel domain (red) at the carboxyl terminus. Disulfides are shown in yellow and calcium ions are shown as green spheres. Each linker subunit exhibits a similar domain structure, with significant differences in the orientation of the amino-terminal long α helix. The extent of each secondary structural element was determined by the program DSSP (Kabsch and Sander, 1983). The amino-terminal ends of the long α helices show the highest mobility and therefore their precise stereochemistry and helical designation is not as accurate as those for the rest of the molecule.

(B) Sequences of the four linker chains (Kao et al., 2006). Alignment was carried out using BOXSHADE. Residues not observed in the crystal structure are shown in italics. Above the sequences are designations of the secondary structural elements (lengths shown are based on the L1 structure) following the color code of (A). Identified directly above the sequences for the α helices are the internal a and d positions of the coiled coils, based on the conventional a–g designations for a heptad repeat. Some residues involved in various contacts are identified below the sequence by the following symbols: p, residues involved in contacts along the P-dyad; q, residues involved in contacts along the Q-dyad; *, L2 and L1 residues involved in an ionic interaction within the triple-stranded coiled coil; h, residues involved in contacts between the linker heterotrimer and the hemoglobin dodecamer.

2000). Each coiled coil connects to its globular head in a disjointed manner as a result of striking differences in disposition of the participant helices from the three linker subunits (Figure 4). Our present electron density maps and refinement, including group B factors, confirm that these segments form α helices, but indicate that they are less well ordered than most of the molecule (Figure 1). (The refined mean B factor for the N-terminal α helices is 103.7 Å^2, whereas the refined mean B factor for the amino acids in the linker head region is 53.7 Å^2.) Such a high mobility does not, however, preclude that an important role for the coiled coils is assembly, particularly in formation of the linker trimer. Rather, this may reflect the disjointed, and perhaps loose, connection between the triple-stranded coiled coil and linker head region.

LDL-A motifs that follow the shorter coiled coils are structurally very similar to other LDL-A motifs (Figure 5), such as the human LR5 domain of the LDL receptor
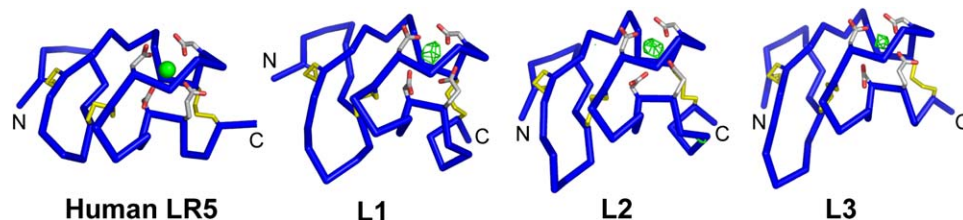

Figure 5. LDL-A Module Structures for the Linker Subunits of *Lumbricus* Erythrocruorin

The α-carbon trace for the LDL-A modules of each linker subunit along with that of the fifth repeat of the human low-density lipoprotein receptor (human LR5) (Fass et al., 1997) is shown in blue, disulfide bonds are shown in yellow, the bound calcium ion for LR5 is shown as a green sphere (at half its van der Waal radius), and the side chains for four acidic residues that are involved in coordinating the calcium ion are shown with carbon atoms light gray and oxygen atoms in red. For the linker subunits, electron density contours are shown in green at the 10σ level (from the 24-fold averaged map) identifying the position of bound calcium ions in each of these domains. Note the similar structure, including identical disulfide linkages and calcium ligating residues, of the LDL-A modules in *Lumbricus* erythrocruorin and the human low-density lipoprotein receptor.

(Fass et al., 1997). The LR5 domain superimposes with the LDL-A motifs of the three unique linker LDL-A domains with rms differences of 1.3–1.4 Å for 35–37 α-carbons. Similarly to that observed in other LDL-A modules, strong electron density is observed for a bound Ca^{2+} ion (12.0–12.5σ in the 24-fold averaged map) in each of the linker subunits.

The C-terminal domain has a typical eight-stranded antiparallel β barrel structure. A structural homology search using DALI (Holm and Sander, 1993) indicated that the second domain of the α subunit of the quinohemoprotein amine dehydrogenase from *Parcoccus denitrificans* (Datta et al., 2001) was most similar (rms differences of 2.5 and 2.7 Å for 101–102 α-carbon pairs with the β barrel domains of L2 and L3, respectively). Differences obtained following superposition of the linker β barrel domains mimic those provided above for linkers: L1 and L2 show rms differences of 1.4 Å for 125 α-carbon pairs, L1 and L3 show differences of 2.4 Å (121 pairs), and L2 and L3 show differences of 2.1 Å (124 pairs). The major differences observed occur in the interstrand loops, which reflect distinct roles of these loops for assembly of the core linker complex.

Linker Heterotrimer
The L1, L2, and L3 linker subunits trimerize. This heterotrimer has a stem, formed from the long triple-stranded coiled coil, and a head region, formed from the short coiled coil, LDL-A, and β barrel domains (Figure 3). The head of the linker trimer provides a quasi-3-fold symmetric surface onto which the 3-fold symmetric dodecamer binds (Figure 3). This quasi-3-fold symmetry is limited to the linker head region due to the disjointed connection between the long and short coiled coils.

The heterotrimeric coiled coils contribute the majority of contacts among the three subunits of the trimeric linker complex. A surface area of 2200–2400 Å^2 is buried from each subunit in the trimer, with more than two thirds of this buried surface contributed by the long and short coiled-coil helices. Additional contacts are formed by the packing of the C-terminal β barrel and LDL-A domains around the periphery of the linker head region (Figure 3).

The extensive interactions among the coiled-coil helices suggest that they may be critical for favoring heteromeric, rather than homomeric, association. The two heterotrimeric coiled coils have canonical arrangements, with nonpolar interactions involving the "a" and "d" positions of the classical heptad repeat. As in other coiled coils, these positions are largely occupied by hydrophobic residues, particularly leucine, isoleucine, and valine (Figure 4). The significant portion of Ile residues at these positions is consistent with formation of trimeric coiled coils (Harbury et al., 1994; Woolfson and Alber, 1995). Substantial variability among the linker sequences at the "a" and "d" positions is evident (Figure 4, labeled "a" and "d") and may contribute to assembly in a heteromeric, rather than homomeric, arrangement. In addition to these nonpolar interactions, some ionic pairs are formed, involving residues at the "e" and "g" positions of the heptad repeat. Three essentially identical ionic pairs occur between Arg 53 and Glu 58 (L1 numbering) on a neighboring subunit that may be important for stabilizing the carboxyl terminus of the second coiled coil.

Within the long coiled coil, an ionic interaction occurs between L2 Arg 52 and L1 Glu 34. Variation in linker sequences at these two positions, designated by asterisks in Figure 4, will promote formation of heteromeric, rather than homomeric, coiled-coil association as a result of charge differences among the linkers at these positions.

One-Twelfth Protomer Structure
The one-twelfth subunit is formed by the binding of a hemoglobin dodecamer to the head of a linker heterotrimer, such that the local 3-fold axis of the dodecamer and the quasi-3-fold axis of the linker globular head region are aligned (Figure 3). Contacts are formed by the outside of the linker trimer head nestling along the irregular outer surface of the dome-shaped hemoglobin dodecamer. As a result, the globular portion of a protomer is hollow, as first identified by cryo-electron microscopic studies (de Haas et al., 1996b, 1997). The LDL-A and β barrel domains of each linker subunit form a contact with one *abc* disulfide-linked trimer within the hemoglobin dodecamer (Figure 6). A substantial interface between the linker heterotrimer and hemoglobin dodecamer is formed, with 3950 Å^2 of the linker trimer surface and 3920 Å^2 of the dodecamer surface buried in this interface. Of this surface area, the β barrel domains contribute ~75% of the linker head buried surface area. For the hemoglobin dodecamer, the hemoglobin b subunits contribute nearly 60% of the buried surface area, with the hemoglobin a subunits contributing roughly 25% and hemoglobin c subunits about 15% of the buried surface area.

Despite an overall quasi-3-fold symmetric arrangement of the hemoglobin dodecamer and linker trimer contact, striking differences in contacting residues are present among the three distinct linker subunits (Figure 4, "h" designates linker residues that contact the hemoglobin dodecamer). One example of this variability involves contacts between the β barrel domain and hemoglobin b subunit. A cluster of aromatic residues, F140, F141, W146, and F170, from L1 dominate the L1-b interaction; however, only F140 and F141 from the BC loop are conserved in the three linker subunits (Figures 4 and 6).

Another illustration of significant variability in the dodecamer-linker interface is found between the linker β barrel domain and its contact with hemoglobin c subunits. The interface between L1 and c shows a peak of strong density (10.5σ in the 24-fold averaged map) that we interpret as a bound calcium ion coordinated by Glu A2 and Asp EF3 from the hemoglobin c subunit along with two main chain carbonyl oxygen atoms from the AB loop of the L1 β barrel domain. (Residues in hemoglobin subunits are identified by helical or corner designation using standard myoglobin nomenclature.) The density level and refinement indicate that this calcium ion is somewhat more weakly bound than the calcium ions bound in the LDL-A modules, but it nevertheless has high occupancy. Additional electron density is also present at the interface between L2 and the second hemoglobin c subunit, but only at the 4σ level, suggesting that a weakly bound calcium ion may be present between L2 and the dodecamer. The equivalent position involving L3 shows no density for a bound calcium, which is consistent with the different conformation of
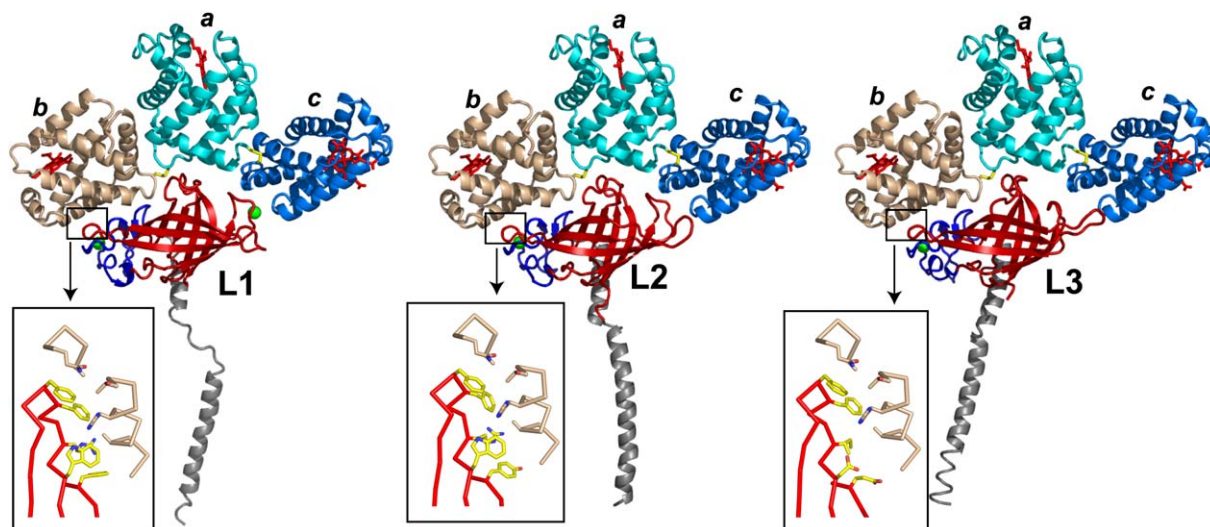
Figure 6. Contacts between Each Linker Subunit and Hemoglobin Subunits

Coloring of hemoglobin subunits and linker domains is the same as in Figure 4. Additionally, disulfides between hemoglobin subunits are shown in yellow and calcium ions are shown as green spheres. Each linker subunit contacts only one disulfide-linked *abc* trimer of the dodecamer. The most extensive contacts involve the β barrel domain of the linker subunits. Despite overall similar interactions, details of the contacts between each linker subunit and the hemoglobin subunits show striking variability. For example, in the insets to the lower left of each overall image, details of the interaction between residues from the BC loop and strand D of each linker subunit with the hemoglobin *b* subunit are shown. Note the variability of the linker residues involved, despite identical binding surfaces on the three hemoglobin *b* subunits. Toward the right of each overall image, differences in the interaction between the linker AB loop of the β barrel domain with a hemoglobin *c* subunit are evident. Within the L1-*c* contact, density for a heavy atom (10.5σ), that we interpret as a calcium ion (green sphere), is clear, whereas much weaker density is observed with the L2-*c* contact and no density is observed for the L3-*c* contact, as the AB loop is significantly different in L3 compared with L1 and L2.

the L3 β barrel AB loop compared with those in L1 and L2 (Figure 6).

Although the surface area contributed by the ∼40 residue LDL-A module is smaller than that from the β barrel domain, an intriguing interaction occurs with the hemoglobin *b* subunit. As shown in Figure 7, Arg B11 from the hemoglobin *b* subunit reaches into the negatively charged calcium binding region of the LDL-A module to make very favorable interactions with Asp 88 (L1 numbering), a conserved residue involved in calcium coordination in all known LDL-A structures. The involvement of residue B11, next to B10 in the ligand binding distal pocket, suggests that this contact could have implications for the oxygen affinity of the hemoglobin *b* subunit. Electrostatic interactions have also been found to mediate contacts involving other LDL-A modules including those within the LDL receptor at endosomal pH (Rudenko et al., 2002) and in a complex between the VLDL receptor and human rhinovirus 2 (Verdaguer et al., 2004). In both cases a Lys, rather than the Arg found here, interacts with the conserved LDL-A residues. Thus, attraction of a basic residue may be an important strategy for the binding of proteins by LDL-A modules. Although the interaction of hemoglobin *b* Arg B11 with the LDL-A acidic residues is very similar in all three linker subunits, other LDL-A residues involved in this contact are not conserved, again illustrating the variability of the contacts between the linker heterotrimer and hemoglobin dodecamer.

Interactions between One-Twelfth Protomers

The linker subunits provide the primary contacts between one-twelfth subunits that create the overall D_6 symmetry found in erythrocruorin. Three distinct contact regions are formed: lateral contacts between neighboring protomers within each hexagonal ring and contacts at two distinct dyad axes, termed P and Q (Figure 2), between protomers on different hexagonal rings.

The lateral contact includes interactions between neighboring hemoglobin dodecamers and interactions between the β barrel domains of L2 and L3 linker subunits. Significant surface area (490 and 540 Å²) is buried at the two surfaces of the interacting linker trimers in the lateral contact; for comparison, 600 and 650 Å² of surface area are buried within each contacting dodecamer. Linker contributions to the lateral contact primarily involve main chain hydrogen bonding between two antiparallel β strands; the beginning of strand D in L3 interacts with the carboxyl end of strand B in L2 (Figure 8), thus extending β sheet hydrogen bonding of the eight-stranded β barrels in subunits L2 and L3. Also contributing to this contact are residues at the very beginning of the β barrel domain of L2, including Lys 126 (three residues prior to strand A) which forms an ionic hydrogen bond (2.7 Å) with L3 Glu 159 at the beginning of strand D.

The most extensive contacts between the two hexagonal layers of erythrocruorin occur along the Q-dyad. These interactions between pairs of protomers involve both linker head contacts and those between the triple-stranded coiled coils, but no contacts involving the hemoglobin subunits (Figure 8). The β barrel domains of L1 subunits from two protomers pack together at the Q-dyad, with each domain burying about 1000 Å² of their surface area in this extensive contact. The contacts include contributions from strands A, B, C, D, and H and neighboring loops (Figure 4, residue positions labeled "q"). The other region of contacts across the Q-dyad occurs at the packing of the long coiled coils
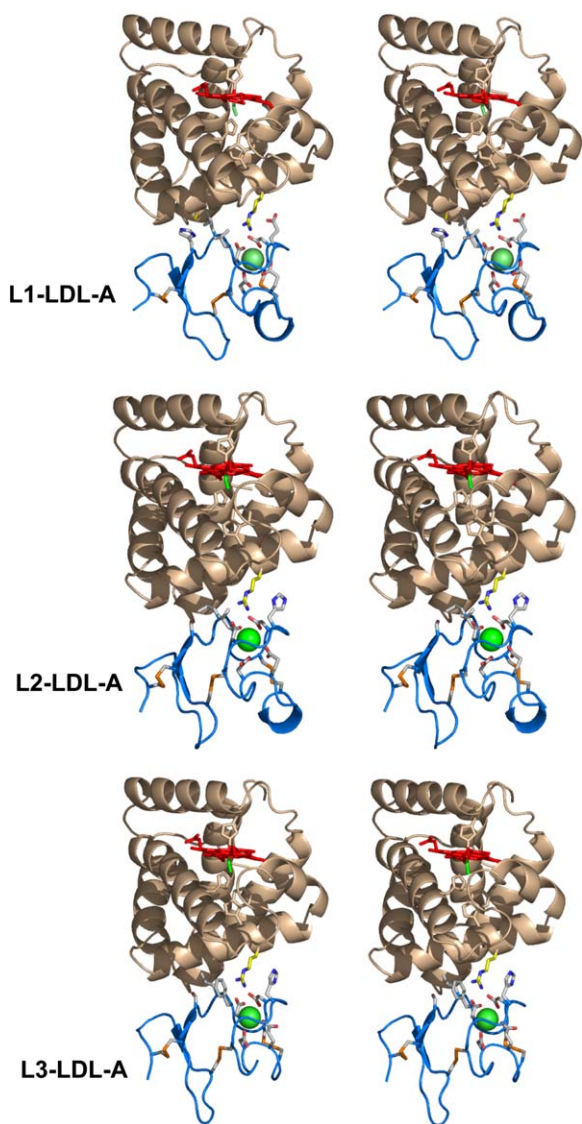
Figure 7. Stereodiagrams of the Interaction between the LDL-A Module and Hemoglobin *b* Subunits

Hemoglobin *b* subunits are shown in light brown with hemes in red and Arg B11 shown with yellow carbon atoms and blue nitrogen atoms, whereas the LDL-A modules are shown in blue with orange disulfides, side chains with gray carbons, red oxygens, and blue nitrogens, and calcium as a green sphere. In this contact, Arg B11 reaches into the heart of the LDL-A module, forming favorable ionic hydrogen bonds with the conserved acidic residues involved in coordinating calcium. The proximity of Arg B11 with the key distal pocket residue Trp B10 suggests that this interaction might impact the oxygen affinity of the hemoglobin *b* subunit. All three LDL-A modules form this same interaction; however, other linker residues involved in the contacts with hemoglobin *b* are variable.

involving the helices from L2 and L3, but not L1. The coiled coils bury about 200 Å^2 from each protomer in the Q-dyad interface.

Contacts along the other unique dyad, the P axis, are much less extensive than those at the Q-dyad, with each protomer burying only 340 Å^2 of surface area. The hemoglobin subunits between the two hexagonal layers have their closest approach at the P-dyad, with amino groups of Lys FG3 from *b* subunits related by the P-dyad about

5.5 Å apart (Figure 2), but this approach is not likely to contribute to assembly. Additionally, the linker head groups are not involved in contacts at the P-dyad. The only actual contacts along the P-dyad occur between the long coiled coils primarily involving L1 subunits. Contacts include Leu 19 from two L1 chains, whose CD1 atoms are 3.2 Å apart and a contact between L1 Tyr 12 CB and L2 Ile 42 CD1, which are 3.7 Å apart. Sequence comparisons (Figure 4, positions labeled "p") show that the homologous residues at these three positions are mostly charged or hydrophilic in the other linker subunits, indicating that similar contacts involving other linker subunits would be unlikely.

Discussion

Erythrocruorins provide large oxygen-carrying capacity in many annelids through their high number of oxygen binding sites per complex and their high in vivo concentration in the blood (Weber and Vinogradov, 2001). The giant size of erythrocruorin (3.6 MDa) is required for vascular retention; however, the blood viscosity in the polychaete annelid *Arenicola marina* is less than 25% of that predicted for a linear polymer of comparable molecular mass (Snyder, 1978), indicating the critical role of erythrocruorin shape in maximizing oxygen transport. We show for *Lumbricus* erythrocruorin that this shape provides 144 oxygen binding sites within a single molecule and is achieved through an intricate series of symmetrical and quasi-symmetrical relationships among its 180 constituent polypeptide chains.

Key to the assembly of *Lumbricus* erythrocruorin is the arrangement of linker subunits that form a central complex. Within each one-twelfth subunit, three distinct linker chains assemble to form a trimeric unit possessing a quasi-3-fold symmetric surface that is complementary to the 3-fold symmetric hemoglobin dodecamer. Despite similar overall structures, the three observed linker subunits exhibit significant local variations. Differences in the linker head region are important for formation of the central linker complex with D$_6$ symmetry; these regions include loop residues in the β barrel domains on L2 and L3 used for lateral contacts and residues on the outer face of the L1 β barrel domains used for contacts at the Q-dyad. Such specialized roles for each linker subunit can only be achieved using trimers containing three different linker sequences. Contributing to heteromeric trimer formation may be the variability of residues involved in coiled-coil packing and residues involved in ionic interactions between neighboring coiled-coil helices. In addition, the contacts of the three distinct linker subunits with the 3-fold symmetric dodecamer are variable, although it is not clear what selective advantage such differences would provide.

Among some annelids, notably the pogonophorans, hemoglobin subunits can assemble into large extracellular respiratory proteins without using linker subunits. Crystal structures reported first of the vestimentiferan *Riftia pachyptila* hemoglobin (Flores et al., 2005) and subsequently of *Oligobrachia mashikoi* hemoglobin (Numoto et al., 2005) show these molecules to have a simpler symmetrical arrangement than the erythrocruorins, with 24 subunits assembling into a 400 kDa spherical assemblage. These structures provide a rationale for the
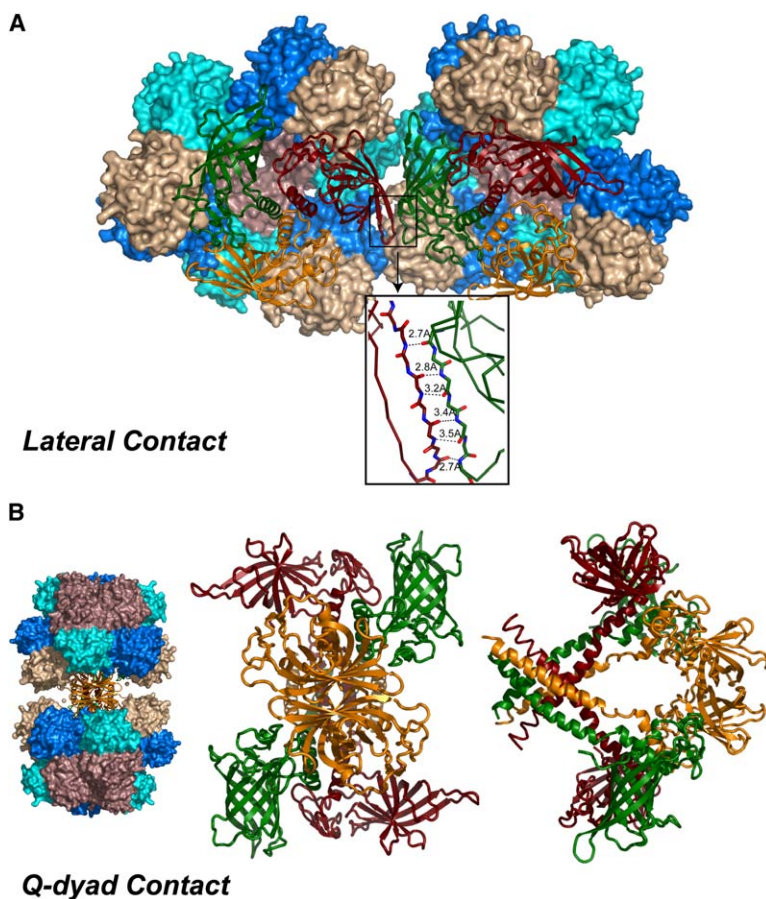
A

Lateral Contact

B

Q-dyad Contact

Figure 8. Contacts between *Lumbricus* Erythrocruorin Protomers

(A) Two one-twelfth units (excluding the long coiled coil) are illustrated, with surface representations of the hemoglobin subunits and colors as in Figure 3, and ribbon diagrams for the three linker subunits with L1 in orange, L2 in green, and L3 in dark red. Contacts are present between neighboring dodecamers, involving two *a* subunits and also *b* subunits packing against *c* subunits. Interactions between linker subunits involve formation of main chain hydrogen bonding between antiparallel β strands from the β barrel domains of L2 and L3, as shown in the inset.

(B) Contacts along the Q-dyad provide the most extensive interactions between the two halves of the molecule. There are no contacts between hemoglobin subunits along the Q-dyad, but extensive packing of the β barrel domains of L1 along with contacts between α helices of L2 and L3 of the triple-stranded coiled coils.

domed shape of the hemoglobin dodecamer found in *Lumbricus* erythrocruorin, as this shape allows two dodecamers to fit tightly together into a hollow D₃ symmetrical spherical assemblage; this suggests that the 400 kDa hemoglobin could represent a first evolutionary step in the development of erythrocruorins (Royer et al., 2005).

Dissociation of dodecamers from *Lumbricus* and other erythrocruorins has been detected in mass spectroscopic experiments (Green et al., 2001). However, such experiments show no evidence for dissociation of *R. pachyptila* 400 kDa hemoglobin into component 200 kDa dodecamers (Flores et al., 2005, online data). These results indicate that the 400 kDa hemoglobin assembly, at least in *R. pachyptila*, is more stable than the interaction between the dodecamer and linker subunits in erythrocruorins, despite forming contacts from similar dodecamer regions in both cases. A possible effect of the weaker contacts in *Lumbricus* erythrocruorin is that these interactions might allow greater ligand-linked quaternary structural changes associated with allosteric transitions in erythrocruorin. Such an idea is consistent with functional data indicating that *Riftia* 400 kDa hemoglobin has reduced Bohr effect and cooperativity in oxygen binding compared with *Riftia* erythrocruorin (Arp et al., 1990).

The assembly and allosteric properties of *Lumbricus* erythrocruorin are regulated by calcium (Fushitani et al., 1986; Zhu et al., 1996). Both very tightly and more weakly bound calcium ions are found in the crystal structure of *Lumbricus* erythrocruorin. The 36 tightly bound calcium ions in the linker LDL-A modules are likely to be important for erythrocruorin assembly. Calcium ions are bound at the interface between linker L1 and hemoglobin *c* subunits, and evidence was found for more weakly bound calcium ions at an equivalent position between linker L2 and hemoglobin *c* subunits. The location of these calcium ions between linker subunits and hemoglobin subunits, whose precise quaternary arrangement is likely to be linked to oxygen binding, suggests the possibility that they may be involved in allostery by contributing to the stabilization of the high-affinity quaternary state. A structural understanding of the calcium role will, however, require elucidation of the ligand-linked structural transitions in erythrocruorin.

The structure presented here reveals unique contributions of each linker subunit to the overall assembly. It is possible, as in the case of some icosahedral viruses, that a single type of linker subunit could suffice if sufficient flexibility were present to allow chemically identical subunits to attain the needed structural differences. In fact, evidence indicates that erythrocruorin molecules can assemble without three distinct linker subunits. Lamy et al. (2000) have shown that molecules that were reassembled using only two types of linker subunits (either L1 and L3 or L1 and L4) can form complexes indistinguishable from native erythrocruorin by cryo-electron microscopy. The reassembly experiments suggest that the unique interactions of L2, such as lateral contacts with L3, can be carried out by L1. Additionally,

the erythrocruorin from the vestimentiferan *Lamellibranchia* is formed using only two types of linker subunits (Suzuki et al., 1989). What selective advantage exists for three (or more) linker subunits? An important consideration is the high concentration of respiratory proteins required for adequate oxygen transport. One possible rationale is that the presence of three (or four) linker paralogs, each involved in unique pairing within the erythrocruorin assemblage, permits more rapid and less error-prone assembly of these megadalton particles. Whereas the need for genetic economy likely drives the evolution of flexibility in viral capsid subunits, genetic economy is not as stringent in this metazoan, permitting development of multiple linker subunits that lead to more efficient assembly than would be possible with a single, more flexible, linker subunit.

Experimental Procedures

Diffraction Data
Crystals of *Lumbricus* erythrocruorin were grown using new conditions from CO-saturated *Lumbricus* erythrocruorin by vapor diffusion against 6% (w/w) PEG 8000, 10 mM $CaCl_2$, 3% isopropanol, 60 mM HEPES (pH 7.5). The crystals were briefly transferred to a stabilizing solution that included 20% PEG 400 and then flash-frozen in a cryostream. Diffraction data from three crystals were collected at BioCARS beamline 14-BMC at the Advanced Photon Source (APS), Argonne National Laboratory, Argonne, IL. These data were processed with HKL2000 and scaled with SCALEPACK (Otwinowski and Minor, 1997). Statistics are provided in Table 1.

Phasing
The starting point for phasing was the 5.5 Å electron density maps obtained in the high-salt crystal form (Royer et al., 2000). The triclinic crystals used here have similar, albeit slightly smaller, cell constants to those used for phasing to 7.25 Å resolution in our earlier study of this molecule (Royer et al., 2000), allowing preliminary positioning of the two molecules per asymmetric unit. Multicrystal molecular averaging using the data from orthorhombic crystals along with the triclinic data led to a map at 5.5 Å resolution that was then used for improvement of the noncrystallographic matrices and molecular envelope. Molecular averaging and improvement of the noncrystallographic matrices was carried out using the RAVE (Kleywegt and Jones, 1994) package of programs. Phasing was then extended from 5.5 Å to 3.5 Å by small increases in resolution using six cycles of 24-fold averaging at each of 50 resolution steps (one additional lattice point along c* for each resolution step). The noncrystallographic matrices and mask envelope were improved using this 3.5 Å map and the phase extension procedure was repeated with these improved matrices and molecular envelope. Final averaging at 3.5 Å resolution led to an averaged map exhibiting an R factor of 27.1% and a correlation coefficient of 0.895 between the observed structure factors and those calculated from this map, portions of which are shown in Figure 1.

Model Building and Refinement
The averaged map was used for fitting models to a one-twelfth unit comprising 12 hemoglobin subunits and three linker subunits using the program O (Jones et al., 1991). Models for the hemoglobin dodecamer based on the refined structure of an isolated dodecamer fit very well to the observed electron density maps and were used as the starting point for the hemoglobin subunits. Starting atomic models for the linker chains were built with the program O (Jones et al., 1991). Five strong isolated density peaks within each one-twelfth unit were observed, in addition to those for the heme iron atoms. Four of these were modeled as calcium ions (discussed in Results) and one zinc ion was modeled associated with the β barrel domain of L2. Atomic models were refined with rounds of minimization and simulated annealing along with group B factors using CNS (Brunger et al., 1998) applying either strict noncrystallographic symmetry or tight noncrystallographic restraints. Refinement of

the one-twelfth molecule using strict 24-fold noncrystallographic symmetry to generate the two whole molecules in the asymmetric unit resulted in conventional and free R factors of 31.7% and 32.2%, respectively. Refinement of the entire structure, by minimization, resulted in lowering these R factors to 28.8% and 29.7%, respectively. Figures were generated with PyMOL (DeLano, 2002).

References

Arp, A.J., Doyle, M.L., Di Cera, E., and Gill, S.J. (1990). Oxygenation properties of the two co-occurring hemoglobins of the tube worm *Riftia pachyptila*. Respir. Physiol. *80*, 323–334.

Bailly, X., Jollivet, D., Vanin, S., Deutsch, J., Zal, F., Lallier, F., and Toulmond, A. (2002). Evolution of the sulfide-binding function within the globin multigenic family of the deep-sea hydrothermal vent tubeworm *Riftia pachyptila*. Mol. Biol. Evol. *19*, 1421–1433.

Brunger, A.T., Adams, P.D., Clore, G.M., DeLano, W.L., Gros, P., Grosse-Kunstleve, R.W., Jiang, J.S., Kuszewski, J., Nilges, M., Pannu, N.S., et al. (1998). Crystallography & NMR system: a new software suite for macromolecular structure determination. Acta Crystallogr. D Biol. Crystallogr. *54*, 905–921.

Caspar, D.L., and Klug, A. (1962). Physical principles in the construction of regular viruses. Cold Spring Harb. Symp. Quant. Biol. *27*, 1–24.

Datta, S., Mori, Y., Takagi, K., Kawaguchi, K., Chen, Z.W., Okajima, T., Kuroda, S., Ikeda, T., Kano, K., Tanizawa, K., and Mathews, F.S. (2001). Structure of a quinohemoprotein amine dehydrogenase with an uncommon redox cofactor and highly unusual crosslinking. Proc. Natl. Acad. Sci. USA *98*, 14268–14273.

de Haas, F., Taveau, J.C., Boisset, N., Lambert, O., Vinogradov, S.N., and Lamy, J.N. (1996a). Three-dimensional reconstruction of the chlorocruorin of the polychaete annelid *Eudistylia vancouverii*. J. Mol. Biol. *255*, 140–153.

de Haas, F., Zal, F., Lallier, F.H., Toulmond, A., and Lamy, J.N. (1996b). Three-dimensional reconstruction of the hexagonal bilayer hemoglobin of the hydrothermal vent tube worm *Riftia pachyptila* by cryoelectron microscopy. Proteins *26*, 241–256.

de Haas, F., Kuchumov, A., Taveau, J.C., Boisset, N., Vinogradov, S.N., and Lamy, J.N. (1997). Three-dimensional reconstruction of native and reassembled *Lumbricus terrestris* extracellular hemoglobin. Localization of the monomeric globin chains. Biochemistry *36*, 7330–7338.

DeLano, W.L. (2002). The PyMOL Molecular Graphics System (http://www.pymol.org).

Dorman, S.C., Kenny, C.F., Miller, L., Hirsch, R.E., and Harrington, J.P. (2002). Role of redox potential of hemoglobin-based oxygen carriers on methemoglobin reduction by plasma components. Artif. Cells Blood Substit. Immobil. Biotechnol. *30*, 39–51.

Fass, D., Blacklow, S., Kim, P.S., and Berger, J.M. (1997). Molecular basis of familial hypercholesterolaemia from structure of LDL receptor module. Nature *388*, 691–693.

Flores, J.F., Fisher, C.R., Carney, S.L., Green, B.N., Freytag, J.K., Schaeffer, S.W., and Royer, W.E., Jr. (2005). Sulfide binding is mediated by zinc ions discovered in the crystal structure of a hydrothermal vent tubeworm hemoglobin. Proc. Natl. Acad. Sci. USA *102*, 2713–2718.

Fushitani, K., Imai, K., and Riggs, A.F. (1986). Oxygenation properties of hemoglobin from the earthworm, *Lumbricus terrestris*. Effects of pH, salts, and temperature. J. Biol. Chem. *261*, 8414–8423.

Fushitani, K., Matsuura, M.S., and Riggs, A.F. (1988). The amino acid sequences of chains a, b, and c that form the trimer subunit of the extracellular hemoglobin from *Lumbricus terrestris*. J. Biol. Chem. *263*, 6502–6517.

Fushitani, K., Higashiyama, K., Asao, M., and Hosokawa, K. (1996). Characterization of the constituent polypeptides of the extracellular hemoglobin from *Lumbricus terrestris*: heterogeneity and discovery of a new linker chain L4. Biochim. Biophys. Acta *1292*, 273–280.

Green, B.N., Gotoh, T., Suzuki, T., Zal, F., Lallier, F.H., Toulmond, A., and Vinogradov, S.N. (2001). Observation of large, non-covalent globin subassemblies in the approximately 3600 kDa hexagonal bilayer hemoglobins by electrospray ionization time-of-flight mass spectrometry. J. Mol. Biol. *309*, 553–560.

Harbury, P.B., Kim, P.S., and Alber, T. (1994). Crystal structure of an isoleucine-zipper trimer. Nature *371*, 80–83.

Harrington, J.P., Gonzalez, Y., and Hirsch, R.E. (2000). Redox concerns in the use of acellular hemoglobin-based therapeutic oxygen carriers: the role of plasma components. Artif. Cells Blood Substit. Immobil. Biotechnol. *28*, 477–492.

Harrison, S.C. (2001). The familiar and the unexpected in structures of icosahedral viruses. Curr. Opin. Struct. Biol. *11*, 195–199.

Hirsch, R.E., Jelicks, L.A., Wittenberg, B.A., Kaul, D.K., Shear, H.L., and Harrington, J.P. (1997). A first evaluation of the natural high molecular weight polymeric *Lumbricus terrestris* hemoglobin as an oxygen carrier. Artif. Cells Blood Substit. Immobil. Biotechnol. *25*, 429–444.

Holm, L., and Sander, C. (1993). Protein structure comparison by alignment of distance matrices. J. Mol. Biol. *233*, 123–138.

Jones, T.A., Zou, J.Y., Cowan, S.W., and Kjeldgaard, M. (1991). Improved methods for building protein models in electron density maps and the location of errors in these models. Acta Crystallogr. A *47*, 110–119.

Kabsch, W., and Sander, C. (1983). Dictionary of protein secondary structure: pattern recognition of hydrogen-bonded and geometrical features. Biopolymers *22*, 2577–2637.

Kao, W.Y., Qin, J., Fushitani, K., Smith, S.S., Gorr, T.A., Riggs, C.K., Knapp, J.E., Chait, B.T., and Riggs, A.F. (2006). Linker chains of the gigantic hemoglobin of the earthworm *Lumbricus terrestris*: primary structures of linkers L2, L3, and L4 and analysis of the connectivity of the disulfide bonds in linker L1. Proteins *63*, 174–187.

Kleywegt, G.J., and Jones, T.A. (1994). Halloween…masks and bones. In From First Map to Final Model, S. Bailey, R. Hubbard, and D.A. Waller, eds. (Warrington, UK: Science and Engineering Research Council Daresbury Lab), pp. 59–66.

Kuchumov, A.R., Taveau, J.C., Lamy, J.N., Wall, J.S., Weber, R.E., and Vinogradov, S.N. (1999). The role of linkers in the reassembly of the 3.6 MDa hexagonal bilayer hemoglobin from *Lumbricus terrestris*. J. Mol. Biol. *289*, 1361–1374.

Lamy, J., Kuchumov, A., Taveau, J.C., Vinogradov, S.N., and Lamy, J.N. (2000). Reassembly of *Lumbricus terrestris* hemoglobin: a study by matrix-assisted laser desorption/ionization mass spectrometry and 3D reconstruction from frozen-hydrated specimens. J. Mol. Biol. *298*, 633–647.

McPherson, A. (1999). Crystallization of Biological Macromolecules (Plainview, NY: Cold Spring Harbor Laboratory Press).

Numoto, N., Nakagawa, T., Kita, A., Sasayama, Y., Fukumori, Y., and Miki, K. (2005). Structure of an extracellular giant hemoglobin of the gutless beard worm *Oligobrachia mashikoi*. Proc. Natl. Acad. Sci. USA *102*, 14521–14526.

Otwinowski, Z., and Minor, W. (1997). Processing of X-ray diffraction data collected in oscillation mode. Methods Enzymol. *276*, 307–326.

Roche, J., Bessis, M., and Thiery, J.P. (1960). Study of the plasmatic hemoglobin of some Annelidae with the electron microscope, in French. Biochim. Biophys. Acta *41*, 182–184.

Royer, W.E., Jr., Strand, K., van Heel, M., and Hendrickson, W.A. (2000). Structural hierarchy in erythrocruorin, the giant respiratory assemblage of annelids. Proc. Natl. Acad. Sci. USA *97*, 7107–7111.

Royer, W.E., Jr., Zhu, H., Gorr, T.A., Flores, J.F., and Knapp, J.E. (2005). Allosteric hemoglobin assembly: diversity and similarity. J. Biol. Chem. *280*, 27477–27480.

Rudenko, G., Henry, L., Henderson, K., Ichtchenko, K., Brown, M.S., Goldstein, J.L., and Deisenhofer, J. (2002). Structure of the LDL receptor extracellular domain at endosomal pH. Science *298*, 2353–2358.

Schatz, M., Orlova, E.V., Dube, P., Jager, J., and van Heel, M. (1995). Structure of *Lumbricus terrestris* hemoglobin at 30 Å resolution determined using angular reconstitution. J. Struct. Biol. *114*, 28–40.

Snyder, G.K. (1978). Blood viscosity in annelids. J. Exp. Zool. *206*, 271–277.

Strand, K., Knapp, J.E., Bhyravbhatla, B., and Royer, W.E., Jr. (2004). Crystal structure of the hemoglobin dodecamer from *Lumbricus erythrocruorin*: allosteric core of giant annelid respiratory complexes. J. Mol. Biol. *344*, 119–134.

Suzuki, T., Takagi, T., Okuda, K., Furukohri, T., and Ohta, S. (1989). The deep-sea tube worm hemoglobin: subunit structure and phylogenetic relationship with annelid hemoglobin. Zoolog. Sci. *6*, 915–926.

Svedberg, T., and Ericksson-Quensel, I.B. (1933). The molecular weight of erythrocruorin. J. Am. Chem. Soc. *55*, 2834–2841.

van Holde, K.E., and Miller, K.I. (1995). Hemocyanins. Adv. Protein Chem. *47*, 1–81.

Verdaguer, N., Fita, I., Reithmayer, M., Moser, R., and Blaas, D. (2004). X-ray structure of a minor group human rhinovirus bound to a fragment of its cellular receptor protein. Nat. Struct. Mol. Biol. *11*, 429–434.

Weber, R.E., and Vinogradov, S.N. (2001). Nonvertebrate hemoglobins: functions and molecular adaptations. Physiol. Rev. *81*, 569–628.

Woolfson, D.N., and Alber, T. (1995). Predicting oligomerization states of coiled coils. Protein Sci. *4*, 1596–1607.

Zal, F., Lallier, F., and Toulmond, A. (2002). Utilisation comme substitut sanguin d'une hemoglobine extracellulaire de poids moleculaire eleve. French patent 00 07031.

Zhu, H., Ownby, D.W., Riggs, C.K., Nolasco, N.J., Stoops, J.K., and Riggs, A.F. (1996). Assembly of the gigantic hemoglobin of the earthworm *Lumbricus terrestris*. Roles of subunit equilibria, non-globin linker chains, and valence of the heme iron. J. Biol. Chem. *271*, 30007–30021.

Accession Numbers

The coordinates of *Lumbricus* erythrocruorin have been deposited in the Protein Data Bank under ID code 2GTL.